Scanning Microscopy Supplement 11, 1997 (Pages 287-300) 0892-953X/97$5.00+.25
Scanning Microscopy International, Chicago (AMF O'Hare), IL 60666 USA

COMPUTER SIMULATION METHODS FOR THE ANALYSIS OF HIGH-ANGLE ANNULAR DARK-FIELD (HAADF) IMAGES OF $Al_XGa_{1-X}As$ AT HIGH RESOLUTION

G. R. Anstis[1]*, S. C. Anderson[2], C. R. Birkeland[2,3] and D. J. H. Cockayne[2]

[1]Department of Applied Physics, University of Technology, Sydney, NSW, Australia
[2] Electron Microscope Unit and Australian Key Centre for Microscopy and Microanalysis, The University of Sydney, NSW, Australia
[3] Department of Physics, Norwegian University of Science and Technology, Trondheim, Norway

Abstract

Quantitative analysis of high-angle, annular, dark-field images formed in a scanning transmission electron microscope requires simulation of the elastic and thermal diffuse scattering of the electron probe. We have implemented two methods for carrying out simulations under the assumption that atomic vibrations are not correlated (the Einstein model). The first method is to determine the average scattering from a number of random configurations of the atoms (the frozen phonon method). The second method calculates thermal diffuse scattering from each atom in turn using a set of atomic scattering functions. The intensity of the scattering from each atom is expressed as a sum of contributions from thermal scattering processes of all orders, each contribution depending on some power of the mean-square atomic displacement of the atom. The purpose of our simulations is to estimate the fraction of Al in the alloy $Al_xGa_{1-x}As$ as a function of distance from an interface between this alloy and GaAs. We compare the amount of computing involved in using the two methods and discuss the accuracies of several approximations. The computations indicate that it should be possible to estimate aluminium fractions with an accuracy of better than 0.1, given a typical signal to noise ratio obtainable in a modern scanning transmission electron microscope.

Key Words: Scanning transmission electron microscopy, dark-field imaging, computer simulation, atomic structure, semiconductor interfaces.

*Address for correspondence:
G.R. Anstis
Department of Applied Physics
University of Technology, Sydney
Broadway, NSW 2007 AUSTRALIA
Telephone number: (61) 02 9514 2193
FAX number: (61) 02 9514 2219
E-mail: Geoff.Anstis@uts.edu.au

Introduction

The scanning transmission electron microscope (STEM) has been used to study the atomic structure of a number of interfaces in crystals. Forming images with electrons which are scattered out to high angles gives a much clearer indication of the abruptness of the interface and mean atomic number of atomic columns than can be obtained through conventional high-resolution microscopy. This approach is known as high-angle, annular dark-field (HAADF) imaging and has been used, for example, by Browning *et al*. (1993) to examine {111} interfaces between $CoSi_2$ and Si, by Jesson *et al*. (1991, 1994) who found unexpected atomic arrange-ments at interfaces in a Si_4Ge_8 ultrathin superlattice and by Jesson *et al*. (1994) who demonstrated that Ge marker layers show up clearly when imaging Si_xGe_{1-x} alloys. The STEM can also be used to carry out high-resolution chemical analysis near the interface by electron energy-loss spectroscopy (Browning *et al*., 1993; Brydson *et al*., 1995).

Computer simulations of the scattering processes leading to image contrast can be employed to obtain quantitative information on the mean atomic number of atomic columns. One detailed study on single crystal InP was undertaken by Hillyard and Silcox (1993). Using a VG HB601UX STEM, we have undertaken a quantitative analysis of an interface between GaAs and $Al_{0.6}Ga_{0.4}As$ and obtained an estimate of the concentration of Al as a function of distance from the interface at a spatial resolution of one monolayer (Anderson *et a*l., 1997).

Several approaches have been developed for simulating image contrast. Wang and Cowley (1990) recognised the importance of thermal diffuse scattering and calculated image intensities using a thermal diffuse scattering function which included first order scattering processes. Pennycook and Jesson (1991) pointed out that contributions from higher order processes are also important and introduced a function which has

contributions from all orders of thermal diffuse scattering. In their study, it is assumed that the atomic scattering function for generating the thermal diffuse scattering is much narrower than the probe. In both works it is assumed that there is no further scattering of diffuse scattering after it has been generated and that each atom vibrates independently of all other atoms (Einstein model). Wang (1995a,b) has shown how his original work can be generalised to include higher-order processes and he has also set out the procedure for including multiple diffuse scattering.

Another approach to simulating scattering is to perform a number of calculations for various static configurations of atoms which are slightly displaced from their mean positions, the amount of displacement depending on the appropriate temperature parameters of the atoms (Loane *et al*., 1991). The dark-field image intensity is then calculated from the average of all the calculations (Xu *et al*., 1991). The scattering is calculated by the Cowley-Moodie multi-slice approach (Cowley, 1981). If Fourier methods are employed, the calculation is for an atomic arrangement that is periodic in the plane perpendicular to the direction of the incident electron beam. The repeat unit (supercell) is chosen to be large enough that all significant intensity of the electron probe is well within the repeat unit. This method of calculating thermal diffuse scattering includes contributions due to elastic scattering of diffuse scattering as well as multiple diffuse scattering. It may be considered the most accurate method of calculating the high-angle scattering, although many computations may have to be carried out to obtain low statistical error. This Monte Carlo approach to calculating the diffuse scattering is often called the frozen phonon method.

Dinges *et al*. (1995) describe an approach which uses a modified transmission function for each atom but also makes use of the Monte Carlo method. The transmission function depends on the temperature parameter of the atom and on a phase factor which can vary at random. Multi-slice calculations are performed for a number of different values of the phase factor for each atom in the supercell and from the average of calculated intensities, an estimate of thermal diffuse scattering is obtained. These calculations assume that multiple diffuse scattering is negligible.

All of the work described above is based on a model of independent atomic vibrations. This assumption may not, however, always be adequate for predicting image contrast. Jesson and Pennycook (1995) showed, by using a model of correlated atomic vibrations due to Warren (1990), that 20% of the effective atomic scattering power of silicon atoms may be due to correlated motion within a column. Treacy and Gibson (1993) have also pointed out the importance of this effect.

In addition to the elastic and thermal diffuse scattering acquired by a high-angle detector, there is the possibility that electrons interacting with a single atomic electron make up a significant proportion of electrons used to form a dark-field image (Bleloch *et al*., 1994).

The present paper investigates the accuracy of a number of approximations to the full calculation of elastic and thermal diffuse scattering and the resulting HAADF image contrast. The full calculations are carried out using two methods, the frozen phonon approach and an approach, described in detail in the next section, based on atomic scattering functions. Since we are interested in high-resolution imaging we confine our studies to thin foils and in particular, because of its relevance to our experimental work (Anderson *et al*., 1997), to (110) foils of $Al_xGa_{1-x}As$ less than 25 nm thick. All of our calculations assume that each atom in the crystal vibrates independently of the other atoms and that the vibrational motion is isotropic. The calculations do not include any inelastic scattering due to excitation of electrons in the foil, since, based on an analysis in the final section of the paper, it is not significant for thin foils. The approximate methods we consider are much faster than the full calculations and we show that they are sufficiently accurate to be useful for estimating the fraction of aluminium within an atomic column from experimental HAADF images.

Our paper is arranged as follows. In the next section we describe two methods for calculating the amount of thermal diffuse scattering. The first method is to apply the frozen phonon approach in conjunction with a slight modification of the Cowley-Moodie multi-slice method. The modification enables efficient generation of the thin phase grating scattering function for each slice of a disordered structure and so speeds up the calculations. The second method is to calculate atomic scattering functions for thermal diffuse scattering. To each atom is associated an infinite set of diffuse scattering functions. These functions are the spatial derivatives of the atomic scattering function and the scattering associated with each function is incoherent with respect to the scattering associated with all the other functions. The total intensity of thermal diffuse scattering is the sum of intensities associated with each type of scattering process.

In the third section we apply these two methods, the frozen phonon method and the use of the scattering functions for the independent thermal diffuse scattering processes, to the calculation of the intensities of HAADF images of $Al_xGa_{1-x}As$. We first show that the two methods lead to similar results and that multiple diffuse scattering is not significant. Then we compare the amount of computing time required for each method. The approach of using a set of atomic scattering functions for thermal diffuse scattering leads to very large calculations since each atom in the foil generates a set of independent waves, each of which propagates to the exit face of the foil and in doing so undergoes both elastic and thermal diffuse scattering.

In the fourth section we investigate the usefulness of a number of approximations for shortening the time for calculations. An important approximation, which is made in most studies using scattering functions, is that there is negligible diffuse scattering if the foil is sufficiently thin. Another approximation is that elastic scattering of diffuse scattering is unimportant if the inner radius of the detector is sufficiently great. Other approximations we investigate are based on calculating the elastic scattering alone or on using the elastic calculation with only one calculation of thermal diffuse scattering. For $Al_xGa_{1-x}As$ we find that intensities can be estimated to within about 5% using some of these approximations.

The final section discusses the relevance of our calculations for estimating the fraction of Al contained within a column of atoms lying along the direction of the incident electrons. We estimate that it should be possible to distinguish fractions differing by 0.1 provided the signal to noise ratio in the image is that achieved under typical operating conditions of a modern STEM. We also briefly discuss why there is no need to consider inelastic scattering from single electrons when estimating the absolute fraction of aluminium.

Calculation of Thermal Diffuse Scattering

In this section we present the theoretical basis for the calculations. Consider a wave travelling in the positive z direction. At the entrance face of a foil the wave function is $\psi_0(\mathbf{R})$, $\mathbf{R}$ being a position vector in the plane perpendicular to the z axis. The wave function is determined by the parameters characterising the objective lens of the scanning microscope. These are C_s (the coefficient of spherical aberration), ε (the amount of defocus), α (the semi-angle of the probe) and parameters characterising fluctuations in source position, electron energy and lens current.

When an electron interacts with an atom the scattered wave can, to a good approximation, be calculated by multiplying the incident wave by the function (Cowley, 1981)

$$\exp[\mathrm{i}\sigma\int_{-\infty}^{\infty}\varphi(\mathbf{R},z)dz] \tag{1}$$

In this equation $\varphi(\mathbf{R},z)$ is the electrostatic potential due to an atom and

$$\sigma = 2\pi me/(h^2k_z) \tag{2}$$

is the interaction constant for high-energy electrons. σ depends on the relativistic mass m and on the z-component of the wave vector $\mathbf{k}$, the magnitude of which is the reciprocal of the relativistic wavelength λ.

We write

$$\bar{\varphi}(\mathbf{R}) = \int_{-\infty}^{\infty}\varphi(\mathbf{R},z)dz \tag{3}$$

for the projected atomic potential.

Consider now an assembly of atoms at positions $(\mathbf{R}_n^{(j)},z_n) \equiv (x_n^{(j)},y_n^{(j)},z_n)$. z_n is the z-coordinate of the nth layer and $z_n < z_{n+1}$. The wave function $\psi_n(\mathbf{R})$ on a plane between z_n and z_{n+1} may be calculated using an approach similar to the multi-slice algorithm of Cowley and Moodie (Cowley, 1981). Given the wave function on a plane before the nth plane, the potential due to the nth plane and the free-electron propagator $p_n(\mathbf{R})$ which describes the propagation of a wave through a distance z_n-z_{n-1}, we may write

$$\psi_n(\mathbf{R}) = \exp[\mathrm{i}\sigma\bar{v}_n(\mathbf{R})]\int p_n(\mathbf{R}-\mathbf{R}')\psi_{n-1}(\mathbf{R}')d\mathbf{R}' \tag{4}$$

The propagator is given by

$$p_n(\mathbf{R}) = \left(\frac{\mathrm{i}k}{z_n - z_{n-1}}\right)\exp\left(\frac{\mathrm{i}kR^2}{z_n - z_{n-1}}\right) \tag{5}$$

and the potential function due to the nth plane of atoms is

$$\bar{v}_n(\mathbf{R}) = \sum_j \bar{\varphi}(\mathbf{R}-\mathbf{R}_n^{(j)}) \tag{6}$$

The exact multi-slice algorithm of Cowley and Moodie requires that the potential be divided into slices of thickness Δz. The wave function is found by calculating the scattering due to a potential slice followed by propagation to the next slice and then scattering by that slice and so on. The exact wave function is obtained by allowing the slice thickness to approach zero. The calculation described by eqation (5) is an approximation to the exact multi-slice algorithm since it does not involve taking the limit of zero slice thickness. However, it is expected to be adequate provided that the range of the atomic potentials in the z-direction is sufficiently small so that the potential between the atomic planes is effectively zero.

It is useful to note that we may write the scattering function for the nth layer in terms of the atomic scattering functions as follows.

$$\exp[i\sigma\bar{v}_n(\mathbf{R})] = \prod_j \exp[i\sigma\bar{\varphi}_n(\mathbf{R}-\mathbf{R}_n^{(j)})] \tag{7}$$

We use this property to calculate the total scattering due to an atomic layer. The atomic scattering functions are stored in arrays. For each different configuration of atoms within a layer, the elements of the arrays are shifted according to the positions of the atoms and the arrays are multiplied together. Thus to generate a

scattering function for a layer with m atoms requires m multiplications of the arrays.

If the foil through which the electrons pass consists of N planes of atoms, the wave function $\psi_N(\mathbf{R})$ can be used to calculate the intensity reaching the detector. If we label points within the diffraction pattern by two-dimensional reciprocal space vectors $\mathbf{U}$, the intensity of the diffracted wave at $\mathbf{U}$ is obtained from the Fourier transform of the wave function $\psi_n(\mathbf{R})$

$$I(\mathbf{U}) = \left| \int \exp[2\pi i \mathbf{U}.\mathbf{R}] \psi_N(\mathbf{R}) d\mathbf{R} \right|^2 \tag{8}$$

and the intensity on the detector is found by summing $I(\mathbf{U})$ over an appropriate range of values of $\mathbf{U}$.

The observed intensities are weighted averages of intensities arising from all possible positions of the atoms. The weightings depend on the amplitudes of atomic vibrations which in turn depend on the temperature. It will be assumed that each atom vibrates independently of all other atoms and that the distribution of deviations in position from the mean is given by the gaussian distribution

$$d(r) = 1/(2\pi\Delta^2)^{3/2} \exp(-r^2/2\Delta^2) \tag{9}$$

where r is a three-dimensional radial coordinate and Δ is the mean squared displacement of an atom in any given direction.

The observed intensity may be found by calculating the intensities for many positions of atoms. This "frozen phonon" model of the interaction of the fast electron with a vibrating lattice can be justified from the fact that the time for the electron to pass through a thin foil is very much less than the periods of vibration of the atoms. The number of configurations of atoms that are required to achieve a given precision in the estimate of image intensities depends on the amplitude of thermal vibrations and on the thickness of the foil.

An alternative approach to calculating observed intensities is to carry out the averaging procedure analytically as far as possible. One calculates average atomic scattering functions, one of which is the elastic scattering function, and the others are thermal scattering functions which involve changes to the vibrational state of the lattice. We now proceed to derive these scattering functions.

Using the distribution of Equation (9) we can calculate the average of the atomic scattering function given in equation (1) for all values of $\mathbf{R}_n^{(j)}$. We work with Fourier transforms.

Let $\Phi(\mathbf{U})$ be the Fourier transform of $\exp[\,i\sigma\overline{\varphi}(\mathbf{R})\,]$ (i.e. the atomic scattering function for a stationary atom) and let $\exp(-\frac{1}{4}Bu^2)$ be the Fourier transform of the distribution function $d(r)$. $\mathbf{u}$ is a three-dimensional reciprocal space vector and

$$B = 8\pi^2\Delta^2 \tag{10}$$

is the standard thermal parameter of crystallography.

We can now calculate an average atomic scattering function which we write as

$$\left\langle \exp[i\sigma\overline{\varphi}(\mathbf{R})] \right\rangle = \int d\mathbf{U} \exp[-2\pi i \mathbf{U}.\mathbf{R}] \Phi(U) \exp(-\tfrac{1}{4}BU^2) \tag{11}$$

This thermally-averaged atomic scattering function can be expressed in terms of $<\overline{\varphi}(\mathbf{R})>$, the thermal average of the projected atomic potential, by introducing a correction potential $i\mu(\mathbf{R})$ (Cowley, 1981).

$$\left\langle \exp[i\sigma\overline{\varphi}(\mathbf{R})] \right\rangle = \exp[i\sigma\{<\overline{\varphi}(\mathbf{R})> + i\mu(\mathbf{R})\}] \tag{12}$$

To calculate the scattering due to a layer containing atoms at mean positions $\mathbf{R}_{eq}^{(j)}$ it is necessary to centre the scattering function on each atomic position. The scattering due to a layer, viz.

$$\prod_j \left\langle \exp[i\sigma\overline{\varphi}(\mathbf{R} - \mathbf{R}_{eq}^{(j)})] \right\rangle \tag{13}$$

is then the input into a standard multi-slice algorithm for the scattering. Note that the average scattering function includes an absorption function due to thermal diffuse scattering so there is no need to use a separate program for calculating corrections to the real potential (Anstis, 1996).

We now consider how thermal diffuse scattering is calculated. With details given in the appendix, we find that atom j in layer n contributes a term

$$\begin{aligned} &\exp[-\tfrac{1}{4}B(\mathbf{V}'-\mathbf{V}'')^2] \exp[2\pi i \mathbf{V}'.\mathbf{R}_{eq}^{(j)}] \Phi(\mathbf{V}') \\ &\times \exp[-2\pi i \mathbf{V}''.\mathbf{R}_{eq}^{(j)}] \Phi^*(\mathbf{V}'') \end{aligned} \tag{14}$$

to the complete multi-slice expression for the intensity at position $\mathbf{U}$ in the detector plane. $\mathbf{V}'$ and $\mathbf{V}''$ are integration variables and there is a pair of such variables for each atom in the foil.

In order to be able to use the multi-slice algorithm we need to be able to work with wave functions only, obtaining intensities by calculating the modulus squared of the wave function that results at the end of the calculation. To achieve this end, we would like to be able to express Equation (14) as a product of a function of $\mathbf{V}'$ and a function of $\mathbf{V}''$. One approach is to write Equation (14) as a sum of such products. Dinges *et al.* (1995) have developed an alternative approach for

achieving this factorisation which is based on a combination of analytical and numerical calculations.

The first exponential term in Equation (14) can be written as the product of three terms: an exponential term with argument depending on V', an exponential term with argument in V'' and $\exp(\frac{1}{2}B\mathbf{V'}.\mathbf{V''})$. The last term can be expanded as a power series in B. Retaining only the first term in this power series, namely 1, we obtain the contribution to the total intensity from the wave which is coherent with the incident beam (elastic scattering). The second term in the series expansion, with B raised to the power one, represents the contribution from single thermal diffuse scattering. This can be seen by noting that in this term factors such as $\mathbf{V'}\Phi(\mathbf{V'})$ occur. This factor is the Fourier transform of the gradient of the atomic scattering function and is related to first-order thermal scattering processes. The term in which B is raised to the power two involves second-order thermal diffuse scattering. Each term in the power series in B corresponds to an independent scattering process, i.e., the different scattering processes are mutually incoherent.

Each independent thermal scattering process can be labelled by two numbers, t and s, with $s \le t$. The Fourier transform of the scattering function for this process is given by

$$T_{s,t}(\mathbf{U}) = \frac{(B/2)^{t/2}}{\sqrt{s!(t-s)!}} U_x^s U_y^{t-s} \Phi(\mathbf{U}) \exp(-\tfrac{1}{4} B U^2) \qquad (15)$$

where U_x and U_y are the x and y components of $\mathbf{U}$.

The complete calculation of thermal diffuse scattering then involves considering all scattering processes, labelled by t and s, for all atoms in the foil. The calculation of elastic scattering involves only the functions $T_{0,0}(\mathbf{U})$ and, as discussed above, it includes the effects of absorption due to thermal diffuse scattering. The scattering functions related to thermal scattering are products of powers of U_x and U_y and the elastic scattering function. Multiplication of a function by powers of U produces a function with significant high-order Fourier components and leads to high-angle scattering of electrons. The larger the value of B the greater is the number of thermal scattering functions that contribute to the intensity of electrons collected by the dark-field detector. Etheridge (1999) has also described how the thermal diffuse scattering can be expressed as a sum of contributions from scattering processes of different orders.

Comparison of Computational Methods

In this section we show that the two methods of calculating high-angle scattering described above produce the same results when used to calculate intensities from [110] foils of $Al_xGa_{1-x}As$. We also consider the amount of computing time required by these methods. In the following section we investigate the usefulness of some approximations to the full scattering calculation, in order to obtain a method for the rapid simulation of dark-field image intensities. Particular interest lies in whether or not good estimates can be obtained from a knowledge of the elastic scattering alone.

A <110> projection of $Al_xGa_{1-x}As$ contains pairs of columns separated by 0.14 nm, one column containing As atoms and the other column containing the other atom types (Fig.1). A rectangular unit cell with two column pairs per cell can be selected. Our calculations use a supercell consisting of 2 x 2 of these unit cells with the potential and wave function sampled at 256 x 256 points. (Calculations which are to be used for the interpretation of experimental images should use a supercell of larger dimensions to accurately model the probe.) Thus for 100 keV electrons all scattering out to 200 mrad is included. The interlayer spacing is 0.3997 nm. The parameters defining the incident probe were: C_s = 1.3 mm (the coefficient of spherical aberration of the VG HB601UX STEM), α = 13.1 mrad, ε = -85.7 nm and a parameter, corresponding to a spread of 20 nm in the focal plane of the objective lens. The introduction of this parameter produces a probe without any rapidly varying oscillations away from the centre. The parameter may be considered as arising from vibrations of the field-emission tip. The value used in these calculations is much greater than for normal operation of a high-resolution microscope. It was chosen to ensure that the probe intensity is zero at the boundary of the supercell. The value of ε used in the calculations gives the sharpest probe for the supercell used. A larger supercell results in an optimum focus close to the theoretical optimum defocus (-69 nm) but the shape is almost the same as that used in our calculations.

Temperature parameters of B_{As} = 0.006853 nm^2 and $B_{Ga} = B_{Al}$ = 0.006373 nm^2 were used.

Calculations were performed for a number of positions within a unit cell. In this paper we concentrate on the 3 points labelled A, B and C in Figure 1. The inner and outer limits of the annular, dark-field aperture were 54 mrad and 150 mrad respectively, these being the values for the VG HB601UX STEM.

Using the Monte Carlo approach, 10 different configurations of the lattice were considered for each position of the probe. This number leads to estimates of the intensity with an uncertainty of less than 4%. Using the atomic scattering function method, convergence was

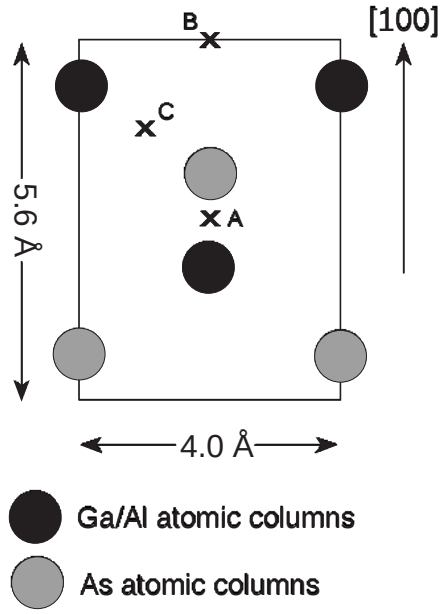

Figure 1. [110] projection of the (Al)GaAs unit cell. Three points A, B and C indicate the probe positions considered in this paper.

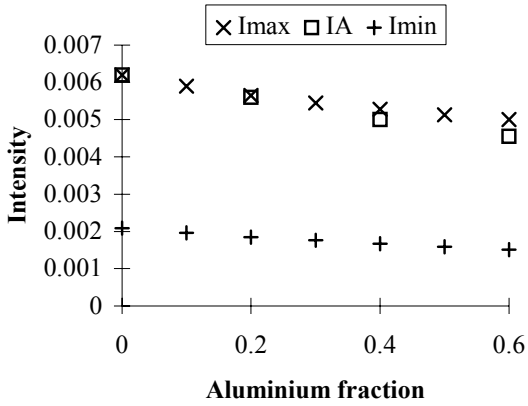

Figure 2. Maximum image intensity and intensities at points A and B (point of minimum intensity) in the unit cell as a function of aluminium concentration for a 20-atom layer foil.

obtained by including all terms up to $t = 6$ in the series expansion of Equation (14). (The $t = 6$ terms contribute about 2% to the total intensity.) It was found to be unnecessary to include double diffuse scattering in these calculations. The results from the two methods agree for a foil thickness of 20 atomic layers (8 nm) for a range of values of the Al fraction x between 0.0 and 0.6. Figure 2 shows intensities at positions A and B and the maximum intensity (which occurs near the As column).

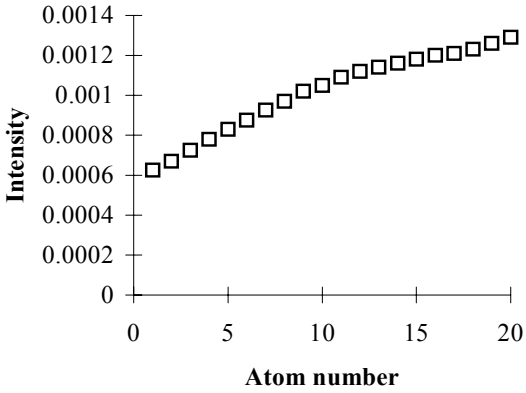

Figure 3. Contribution of each As atom in a column to the total diffuse scattering. The probe is at position A and the column is the closest As column.

We finish this section with a brief discussion of the amount of computing required by each of the two methods. To achieve an accuracy of 1% with the Monte Carlo approach about 25 configurations of atoms are necessary. Thus the computational time required is thetime to run 25 standard multi-slice calculations plus some small additional time to generate the scattering function for each slice. As indicated in the discussion following equation (7) the scattering function can be generated efficiently by shifting and multiplying arrays of atomic scattering functions for elastic scattering. On the other hand the approach of using thermal scattering functions, using all terms up to $t = 6$, requires, for each atom in the cell, 28 multi-slice calculations from the layer containing the atom to the exit face of the foil. Assuming that on average the number of layers per calculations is half the number of layers making up the foil, 14 standard multi-slice calculations are required per atom in the foil. For a foil consisting of 20 layers with 16 atoms per layer around 9000 multi-slice calculations are required, considerably more than required by the Monte Carlo method, to produce the intensity at just one point within the unit cell.

Approximations

We have investigated some ways of reducing the times of carrying out computations which use atomic thermal scattering functions. To begin with we considered that it may be sufficient to calculate the diffuse scattering from atoms in only a few layers and to determine the contributions from atoms in the other layers by interpolation.

Figure 3 shows that this approach should give good accuracy. It shows the contributions to the total dark-field intensity due to each atom in the As column when the probe is at position A. The contribution of an atom depends on the probe intensity which varies with depth

in the foil and on the amount of rescattering of diffuse scattering to angles outside the acceptance angles of the detector. While the calculation time is reduced by using interpolation, it is still, however, considerable.

Another approximation is to consider that the total scattering can be calculated by assuming that once thermal diffuse scattering has occurred no further scattering of the diffuse scattering takes place (Pennycook and Jesson, 1991; Wang, 1995a). We found that this approximation gives an accuracy of better than 5% for a foil consisting of 20- atom-layers. The amount of computing using this approximation is relatively small. It requires only one multi-slice calculation and 20 x 28 complex multiplications to generate the diffuse scattering (taking t = 6 as in the example of the previous section).

We consider next two approximations based on the assumption that the total scattering can be estimated from calculations based on the theory of elastic scattering so that no calculation of thermal diffuse scattering is required. It is assumed that the total scattering into the detector is proportional to the elastic scattering into the detector and that the elastic scattering is calculated: (1) with absorption due to atomic vibrations taken into account and (2) without absorption.

Figure 4 shows how the intensity of elastic scattering into the detector expressed as a fraction of the total scattering into the detector, calculated with the effects of thermal diffuse scattering included, varies as a function of number of atomic layers. In Figure 4a the elastic scattering is calculated assuming there is absorption due to atomic vibrations. It shows that most of the electrons reaching the high-angle detector have undergone thermal diffuse scattering.

In Figure 4b the elastic scattering is calculated without absorption, i.e. atoms are assumed to be stationary while the total scattering is calculated without any approximations. A fraction less than 1 shows that the angular distribution of thermal diffuse scattering, being dependent on the spatial derivatives of the atomic scattering function, is different from the scattering due to a single atom.

The calculations summarised in these figures show that the image intensity can be calculated from the elastic scattering alone to an accuracy of about 10% when absorption is included and to about 5% when no absorption is included in the calculation of the elastic scattering.

Another approximation is to assume that the total scattering into the detector is proportional to a fraction of the total amount of thermal diffuse scattering plus the elastic scattering into the detector. This assumption can be stated as

$$I_{DF} = I_{DF}^{elastic} + \beta(1 - I_{TOTAL}^{elastic}) \qquad (16)$$

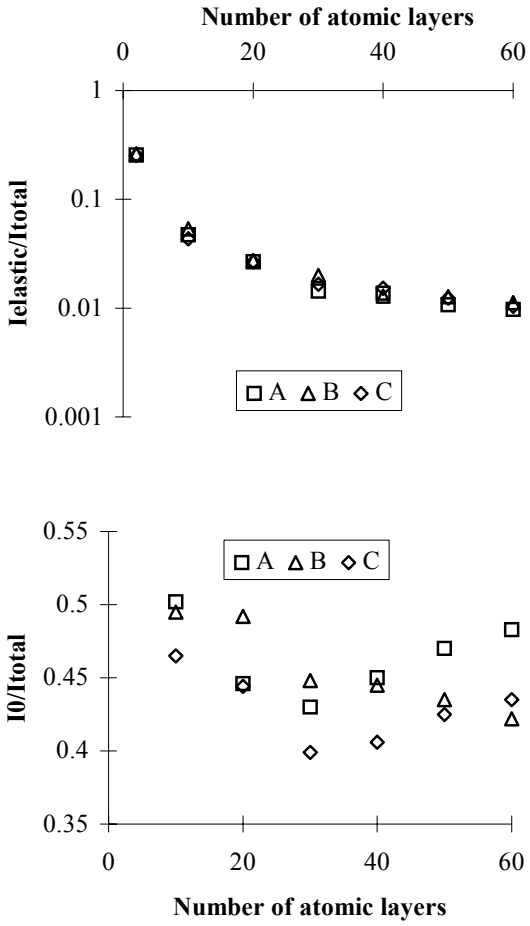

Figure 4. (**a**) The contributions to the intensities at points A, B and C due to elastically scattered electrons for different numbers of atomic layers. The contributions are expressed as fractions of the dark-field intensities calculated without approximation and are made assuming vibrating atoms. (**b**) The dark-field image intensities at points A, B and C, calculated assuming stationary atoms, expressed as a fraction of the intensity calculated using a full calculation.

where $1 - I_{TOTAL}^{elastic}$ is the total thermal diffuse scattering.

Figure 5 shows the predictions of the value of β based on equation (16). The error bars are a consequence of using the frozen phonon method with a finite number of atomic configurations. We observe that if β is estimated from the intensity at point A of an image of a thin foil, we can predict intensities at other points in the unit cell with an accuracy better than 5% for foils of thickness 10 layers to 60 layers. Calculations performed by Anderson *et al*. (1997) using the scattering function method to estimate diffuse scattering show that for a foil consisting of 20-atom layers, estimating β from one point of the image

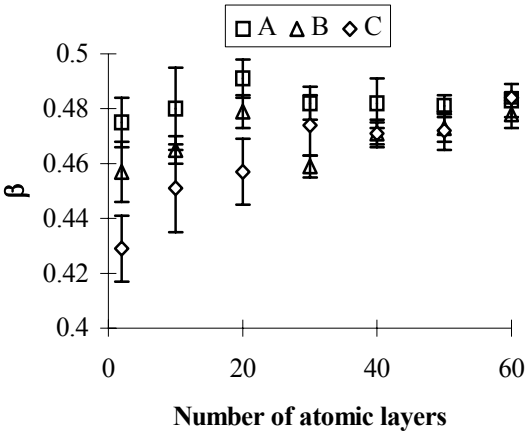

Figure 5. The parameter β for three positions in the unit cell as a function of the number of atomic layers.

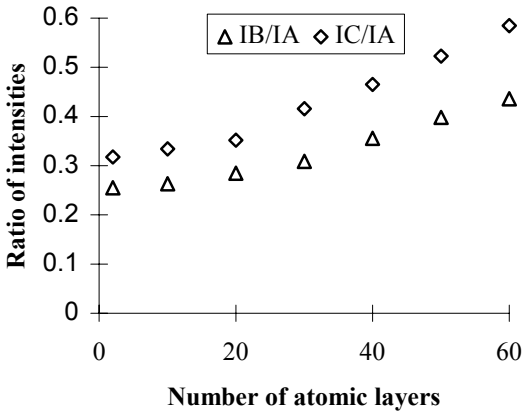

Figure 6. The intensities at points *B* and *C* expressed as fractions of the intensity at point *A* for different numbers of atomic layers.

can be used to find the intensities at other points with an accuracy of 1%. This figure is not inconsistent with the results of Figure 5 when allowance is made for the statistical errors associated with the Monte Carlo method.

The last approximation for reducing calculation times that we considered in detail is that relative intensities of an image of a thick foil can be calculated from a knowledge of the relative intensities of an image of a thin foil.

From Figure 6, which shows how the fractions I_B/I_A and I_C/I_A change with the number of atomic layers, it is seen that the relative intensities change by no more than 10% for foils less than 20 layers thick, but for thicker foils the fractions are greater which corresponds to reduced image contrast. This reduction is due to the strong attenuation of a probe, centred on a column of atoms, after it has interacted with several atoms. Thus the rate of scattering through high angles, being approximately proportional to the intensity of the probe, is reduced in thicker regions of the foil.

There are some other approximate methods which we have not investigated. One is to use incoherent imaging theory which states that the image intensity is the convolution of a probe intensity function with an object scattering function which depends on the thickness of the foil. Loane *et al*. (1992) showed that this theory correctly predicts the variation of the intensities of fringes in images of InP due to changes in the focussing of the objective lens. Incoherent imaging theory provides no advantage in computing time for a single value of objective lens defocus, since to find the object scattering function requires calculation of the thermal diffuse scattering.

Another approximate method of calculating image contrast, which should be assessed, is to assume that the atomic scattering functions for thermal scattering are much more localised in real space than is the wave function for the atom probe (Pennycook and Jesson, 1991). Then, assuming there is no further scattering of thermal diffuse scattering, the intensity of scattering to position U in reciprocal space due to an atom centred at position x_n is

$$I(\mathbf{U}) = \sum_{s=1}^{\infty}\sum_{t=0}^{s}\left|T_{s,t}(\mathbf{U})\right|^2 I(x_n) + I^{elastic}(\mathbf{U})$$
$$= \left|\Phi(\mathbf{U})\right|^2\left(1-\exp[-\tfrac{1}{2}BU^2]\right)I(x_n) + I^{elastic}(\mathbf{U}) \quad (17)$$

where $I(x_n)$ is the intensity of the probe at the position of the atom. In this expression the elastic scattering is calculated according to coherent imaging theory. The dark-field intensity is determined from this equation by integrating over all values of U corresponding to the angular range of the detector. Typically the contribution of the elastic scattering to the total intensity is small and so is not included in estimating the dark-field intensity (Pennycook and Jesson, 1991). Use of this approxi-mation will lead to a small decrease in computing time compared with calculations based on using a finite set of the scattering functions given by equation (15) since in both methods most of the computation involves calculating the wave function for an elastically scattered electron. The approximation does have the advantage of requiring less computer memory because only the elastic scattering function needs to be stored.

There are also approximations to the full Monte Carlo calculations which could be considered. If the assumption that diffuse scattering is not significantly rescattered is applicable, the image intensity can be found by calculating the elastic scattering, with absorption due to thermal diffuse scattering taken into account, to a certain depth within the foil and then

generating thermal diffuse scattering by averaging the scattering due to random configurations of atoms within one slice. This approximation would result in significant reductions in computing time since only one multi-slice calculation is required for each position of the probe. Based on the results presented above, this approximation should have an accuracy of about 5%.

Estimating the Al Fraction

Figure 2 indicates that image contrast, defined by

$$C = \frac{I_{\max} - I_B}{I_{\max} + I_B} \qquad (18)$$

changes from 0.50 to 0.54 as x changes from 0.0 to 0.6. I_{max}/I_B changes from 3.0 to 3.3 with the same change in x. These are changes of about 10%. On the other hand, the absolute intensity at any given point within the unit cell decreases by approximately 20% in going from $x = 0$ to $x = 0.6$. A consideration of the maximum intensity is one of the methods used by Anderson *et al*. (1997) to estimate the Al fraction across an interface between GaAs and $Al_{0.6}Ga_{0.4}As$. They also considered the distribution of intensities (i.e., the shape) within an image of a unit cell, since this depends on x. Figure 2 shows how the difference in the maximum intensity and the intensity between a pair of closely spaced columns (point A) varies with x. As the aluminium fraction increases from 0, the position of the maximum intensity moves away from point A towards the As column.

To obtain an indication of the precision with which x can be measured using HAADF images, consider the method of estimation based on measuring the maximum intensity in the image. In order to distinguish regions differing in the Al fraction by an amount 0.1, the maximum intensity in the unit cell must be estimated with a precision of better than about one sixth of 20%, i.e. 3%. Variations in intensity in an experimental HAADF image are around 25% (Anderson *et al*., 1997). This estimate comes from considering the digitally recorded intensities at equivalent points in a row of unit cells parallel to the interface. The variation is greater than that expected from shot noise alone so factors such as surface contamination, radiation damage and charging effects must be involved. The resolution of the VG HB601UX STEM is about 0.3 nm so that the intensity in a noise-free image should not vary significantly in an area 0.05 nm x 0.05 nm. If an experimental digitised image of this area consists of 9 x 9 pixels and there is a variation in intensity of 25% among the pixels, the mean intensity should be an estimate of the noise-free intensity with a precision of about 3%, assuming that the precision is inversely proportional to the square root of the number of measurements and that the intensity variations are uncorrelated. In the experimental work of Anderson *et al*. (1997), each pixel corresponds to a region of dimensions 0.017 nm x 0.017 nm which is an insufficient frequency of sampling for estimating x to within 0.1 for a single cell. Given this limitation, these authors used the maximum intensity to estimate an average value of x for a number of cells lying parallel to the interface and in this way were able to obtain estimates of x for varying distances from the interface which have a precision better than 0.1.

If instead of the maximum intensity, the mean intensity of an image of a unit cell is used to estimate the fraction of aluminium, the change in intensity is only 10% over the range of values of x but many more pixels per unit cell are available. With 33 x 24 pixels per unit cell and with the amount of intensity variation as before, it should be possible to estimate the mean intensity with a precision of 1%, which is sufficient to estimate the aluminium fraction in any unit cell with a precision of 0.1. This analysis assumes that errors in the measured experimental intensities are not correlated, an assumption which may not be true and requires further investigation.

Both of these methods, being based on one number for each unit cell to estimate x, are susceptible to errors due to unknown variations in the thickness of the foil. A method which uses the shape of the image is more reliable and is discussed in detail by Anderson *et al*. (1997).

The above considerations show that image simulations play an important role in experimental design and in the quantitative analysis of images.

The methods of calculating intensity which are described in the earlier sections are based on the assumption that only elastic and thermal diffuse scattering is significant. Bleloch *et al*. (1994) suggested that inelastic scattering by single electrons may be important. We now provide a rough estimate of the significance to HAADF intensities of this scattering mechanism.

A simple model of inelastic scattering through large angles holds that the ratio of inelastic to elastic scattering equals the inverse of the atomic number of the atom. (Reimer, 1984). Under this assumption high-angle, inelastic scattering for both As and Ga is about 1/30 th the elastic scattering for these atoms while for Al the fraction is 1/13. Since for a 20-atom-layer foil the elastic scattering contributes only about 3% to the total flux onto the annular detector, the effects of inelastic scattering should be insignificant.

In conclusion we have shown that the theoretical tools for quantitative analysis of HAADF images of simple structures are available. For the system considered in this paper, it does not appear to be necessary to carry out the full calculation of thermal diffuse scattering by, for example, using Monte Carlo

methods, since good approximations to the full calculations are available. The assumption that elastic scattering of thermal diffuse scattering produces only a rearrangement of the diffuse scattering within the angular range accepted by the dark-field detector is adequate. A numerical method for calculating the diffuse scattering based on this assumption has been given. It is equivalent to methods proposed by other authors and requires similar computing times to these methods. Some other equally suitable approximations have been given. In this paper the Einstein model of independent atomic vibrations has been used. It may be difficult to generalise the method employed in this paper to include correlated atomic motions since the thermal scattering functions for individual atoms are derived assuming vibrational independence. The methods of Jesson and Pennycook (1995) and Wang (1995b) may be more suitable for investigating the importance of this effect.

Appendix

Equation (14) is derived from equations (4) and (7). Equation(4) implies

$$\begin{aligned}\psi_{n+1}(\mathbf{R}) &= \exp[\mathrm{i}\sigma\bar{v}_{n+1}(\mathbf{R})] \\ &\times \int d\mathbf{R}'\, p_{n+1}(\mathbf{R}-\mathbf{R}')\exp[\mathrm{i}\sigma\bar{v}_n(\mathbf{R}')] \\ &\times \int d\mathbf{R}''\, p_{n+1}(\mathbf{R}'-\mathbf{R}'')\psi_{n-1}(\mathbf{R}'')\end{aligned} \tag{19}$$

Using equation (7) and retaining only those terms involving $\mathbf{R}_n^{(j)}$ and z_n we are led to consider

$$\begin{aligned}&\int d\mathbf{R}'\, p_{n+1}(\mathbf{R}-\mathbf{R}')\exp[\mathrm{i}\sigma\bar{\varphi}(\mathbf{R}-\mathbf{R}_n^{(j)})] \\ &\times \int d\mathbf{R}''\, p_{n+1}(\mathbf{R}'-\mathbf{R}'')\psi_{n-1}(\mathbf{R}'')\end{aligned} \tag{20}$$

Introducing $\Phi(U)$, the Fourier transform of $\exp[\,\mathrm{i}\sigma\bar{\varphi}(\mathbf{R})\,]$, we can express equation (20) as

$$\begin{aligned}&\int d\mathbf{R}' \int d\mathbf{U}' \exp[-2\pi\mathrm{i}\mathbf{U}'.(\mathbf{R}-\mathbf{R}')]P_{n+1}(\mathbf{U}') \\ &\times \int d\mathbf{V}' \exp[-2\pi\mathrm{i}\mathbf{V}'.(\mathbf{R}'-\mathbf{R}_n^{(j)})]\Phi(\mathbf{V}') \\ &\times \int d\mathbf{R}'' \int d\mathbf{W}' \exp[-2\pi\mathrm{i}\mathbf{W}'.(\mathbf{R}'-\mathbf{R}'')]P_n(\mathbf{W}')\psi_{n-1}(\mathbf{R}'')\end{aligned} \tag{21}$$

where

$$P_n(\mathbf{U}) = \exp[-\mathrm{i}\pi\lambda U^2(z_n - z_{n-1})] \tag{22}$$

is the Fourier transform of the propagator.

The integration with respect to $\mathbf{R}'$ produces a delta function $\delta(\mathbf{U}' - \mathbf{V}' - \mathbf{W}')$. Integration with respect to $\mathbf{U}'$ and using equation (22) gives

$$\begin{aligned}&\int d\mathbf{V}' \int d\mathbf{W}' \exp[-2\pi\mathrm{i}(\mathbf{V}'+\mathbf{W}').\mathbf{R}] \\ &\times \exp[-\pi\mathrm{i}\lambda(\mathbf{V}'+\mathbf{W}')^2(z_{n+1}-z_n)]\exp[2\pi\mathrm{i}\mathbf{V}'.\mathbf{R}_n^{(j)}]\Phi(\mathbf{V}') \\ &\times \int d\mathbf{R}'' \exp[2\pi\mathrm{i}\mathbf{W}'.\mathbf{R}'']\exp[-\pi\mathrm{i}\lambda W'^2(z_{n+1}-z_n)]\psi_{n-1}(\mathbf{R}'')\end{aligned} \tag{23}$$

We are interested in determining the intensity of the electron wave and so we multiply the above expression by a similar one involving complex conjugates. There are two new integration variables $\boldsymbol{V''}$ and $\boldsymbol{W''}$ in the resulting expression. The weighted average of this expression, considered as a function of $\mathbf{R}_\mathbf{n}^{(\mathbf{j})}$ and z_n, is obtained by performing a convolution with the distribution equation (9), which gives the probability of an atom being displaced a certain distance from its equilibrium position. Averaging first over the values of $\mathbf{R}_\mathbf{n}^{(\mathbf{j})}$ we obtain the terms

$$\begin{aligned}&\exp[-\tfrac{1}{4}B(\mathbf{V}'-\mathbf{V}'')^2]\exp[-\mathrm{i}\pi\lambda(\mathbf{V}'+\mathbf{W}')^2(z_{n+1}-z_n)] \\ &\times \exp[2\pi\mathrm{i}\mathbf{V}'.\mathbf{R}_{eq}^{(j)}]\Phi(\mathbf{V}')\exp[-\mathrm{i}\pi\lambda W'^2(z_n - z_{n-1})] \\ &\times \exp[\mathrm{i}\pi\lambda(\mathbf{V}''+\mathbf{W}'')^2(z_{n+1}-z_n)] \\ &\times \exp[-2\pi\mathrm{i}\mathbf{V}''.\mathbf{R}_{eq}^{(j)}]\Phi^*(\mathbf{V}'')\exp[\mathrm{i}\pi\lambda W''^2(z_n - z_{n-1})]\end{aligned} \tag{24}$$

where $\mathbf{R}_{eq}^{(j)}$ is the mean position of atom j in layer n.

Then, averaging over all values of z_n, we obtain

$$\begin{aligned}&\exp[-\tfrac{1}{4}B(\mathbf{V}'-\mathbf{V}'')^2]P_{n+1}(\mathbf{V}'+\mathbf{W}') \\ &\times \exp[2\pi\mathrm{i}\mathbf{V}'.\mathbf{R}_{eq}^{(j)}]\Phi(\mathbf{V}')P_n(\mathbf{W}') \\ &\times P_{n+1}^*(\mathbf{V}''+\mathbf{W}'')\exp[-2\pi\mathrm{i}\mathbf{V}''.\mathbf{R}_{eq}^{(j)}]\Phi^*(\mathbf{V}'')P_n^*(\mathbf{W}'') \\ &\times \exp\{-\tfrac{1}{16}B\lambda^2[(\mathbf{V}'+\mathbf{W}')^2 - W'^2 - (\mathbf{V}''+\mathbf{W}'')^2 + W''^2]^2\}\end{aligned} \tag{25}$$

In this equation terms such as $P_n(\mathbf{W}')$ are calculated assuming the average value of z_n.

Equation (14) consists of those terms in equation (25) related to scattering by atom j in layer n but does not include terms relating to the propagation of the wave between slices. When the multi-slice calculation is carried out the propagators are included but the last exponential in the above equation is approximated by 1. The absolute error in making this approximation is not large for a value of the argument which is typical for high-energy scattering. The processes neglected by making this approximation are related to the effects on the thermal diffuse scattering due to the variations in the separations of layers.

References

Anderson SC, Birkeland CR, Anstis GR, Cockayne DJH (1997) An approach to quantitative compositional profiling at near-atomic resolution, Ultramicroscopy (in press).

Anstis GR (1996) Corrections to atomic scattering factors for high energy electrons arising from atomic vibrations. Acta Cryst **A52**: 450-454.

Bleloch AL, Castell MR, Howie A, Walsh CA (1994) Atomic and electronic Z-contrast effects in high-resolution imaging. Ultramicroscopy **54**: 107-115.

Browning ND, Chisolm MF, Pennycook SJ (1993) Atomic-resolution chemical analysis using a scanning transmission electron microscope. Nature **366**: 143-146.

Brydson R, Bruley J, Mullejans H, Scheu C, Ruhle M (1995) Modelling the bonding at metal-ceramic interfaces using PEELS in the STEM. Ultramicroscopy **59**: 81-92.

Cowley JM (1981) Diffraction Physics 2nd ed. (North Holland, Amsterdam), Chapter 12.

Dinges C, Berger A, Rose H (1995) Simulation of TEM images considering phonon and electronic excitations. Ultramicroscopy **60**: 49-70.

Etheridge J (1999) High-resolution electron-micros-cope images of crystals with correlated atomic displacements. Acta Cryst. **A55**: 143-159.

Hillyard S, Silcox J (1993) Thickness effects in ADF STEM zone axis images. Ultramicroscopy **52**: 325-334.

Jesson DE, Pennycook SJ (1995) Incoherent imaging of crystals using thermally scattered electrons Proc R Soc Lond **A449**: 273-293.

Jesson DE, Pennycook SJ, Baribeau J-M (1991) Direct imaging of interfacial ordering in ultrathin $(Si_mGe_n)_p$ superlattices. Phys Rev Lett **66**: 750-753.

Jesson DE, Chisholm MF, Pennycook SJ, Baribeau J-M (1994) Ordered structures at Si on Ge(001) Interfaces. Phys Rev Lett **75**: 184.

Loane RF, Xu P, Silcox J (1991) Thermal vibrations in convergent-beam electron diffraction. Acta Cryst **A47**: 267-278.

Loane RF, Xu P, Silcox J (1992) Incoherent imaging of zone axis crystals with ADF STEM, Ultramicroscopy **40**: 121-138.

Pennycook SJ, Jesson DE (1991) High-resolution Z-contrast imaging of crystals. Ultramicroscopy **37**: 14-38.

Reimer L (1989) Transmission Electron Microscopy. Springer, Heidelberg. p 159.

Treacy MMJ, Gibson JM (1993) Coherence and multiple scattering in "Z-contrast" images. Ultramicroscopy **52**: 31-53.

Wang ZL, Cowley JM (1990) Dynamic theory of high-angle annular-dark-field STEM lattice images for a Ge/Si interface. Ultramicroscopy **32**: 275-289.

Wang ZL (1995a) Elastic and Inelastic Scattering in Electron Diffraction and Imaging. Plenum, New York. Chapter 11.

Warren BE (1990) X-ray Diffraction. Dover, New York.

Wang ZL (1995b) Dynamical theories of dark-field imaging using diffusely scattered electrons in STEM and TEM. Acta Cryst **A51**: 569-585.

Xu P, Loane RF, Silcox J (1991) Energy-filtered convergent-beam electron diffraction in STEM. Ultramicroscopy **38**: 127-133.

Discussion with Reviewers

Z.L. Wang: The paper by Pennycook and Jesson (1991) considers that the image contrast in HAADF is simply a convolution of the probe shape with an object scattering function, and they concluded that no simulation is needed for image interpretation. This theory does not consider any beam broadening and dynamical scattering in HAADF STEM imaging. From your calculation how important is the dynamical scattering in HAADF imaging? How important do you think the calculation is for quantitative HAADF image analysis? Does the conclusion still hold for grain boundary imaging?

M. Hÿtch: For the measurement of the aluminium concentration, have the authors considered the non-local effects, i.e., the probe spreading onto neighbouring columns thus averaging the measure?

Authors: Dynamical scattering is important since it determines how the intensity within the probe is redistributed by the atomic columns. We investigated the effects of beam broadening and found that even for foils 20 atoms thick the contribution to the thermal diffuse scattering from columns away from the centre of the probe increases with increasing thickness. We have not attempted a comparison between a calculation which assumes the probe is not modified by the atoms and the full calculation so we cannot say how accurate the simpler calculations may be for estimating aluminium concentrations. Our calculations are based on perfect crystals with a given fraction of aluminium. Thus if beam spreading is important our calculations may be in error when the probe is very close to the interface.

Z. L. Wang: Diffuse scattering can be generated either by TDS or by short-range ordering of point defects (i.e., static displacement), such as point vacancies, differences in atomic sizes, lattice relaxation and strain. The last, however, was not included in your calculations. In analysis of $Al_xGa_{1-x}As$ using HAADF STEM images, how much contrast can the lattice introduce as a result of atom substitution of Ga by Al?

J. M. Gibson: What is the role of static displacements in the contrast, especially in the accuracy

of composition method? I am thinking particularly of the old work of Hall and Hirsch on these effects.

Authors: We have not investigated the issue of strain directly. If the effect of point defects can be modelled by introducing an effective Debye-Waller factor then we believe our results are not much affected since the temperature parameters for the atomic species in the alloy are not known and it was necessary to show that the estimated atomic fractions did not change significantly for a range of atomic thermal parameters.

Z. L. Wang: I am not quite ready to accept the argument described at the end of the paper about the contribution of single electron excitation to HAADF images (Bleloch *et al*., 1994). The fine atomic-scale details in HAADF images may not be affected by Compton scattering, because the width of the Compton peak observed in EELS spectra is usually more than 50-100 eV, and the fine details, if any, from Compton scattering may be washed out. Thus this scattering process may only introduce a background in the image. If the image background is set digitally in STEM, this process eventually does not affect the displayed image contrast.

Authors: Thank you for these comments.

Z. L. Wang: What are the advantages and disadvantages of your methods compared with those reported in the literature?

Authors: The advantage of the series approach outlined in this paper is that the accuracies of certain approximations can be checked. On the other hand if no approximations are possible, the approach leads to extremely long calculations compared with the Monte-Carlo approach. The method also has the disadvantage that correlated atomic vibrations are not easily incorporated into the formalism.

P. D. Nellist: To what extent do the authors consider the accuracy of the determined composition to be limited by the independent oscillator model of the phonons? Would a more physical phonon model with vibrational correlations between neighbouring atoms give a different result?

Authors: The results of Jesson and Pennycook (1996) using the Debye model suggest that differences in absolute image intensities are as large as 20%. If relative intensities are not so dependent on the degree of vibrational correlations, and this should be further investigated, then the present calculations can be used to estimate composition from an analysis of experimental images.

A. Howie: If intensities are to be compared at various points in the unit cell, it might have seemed more obvious to compare the intensity on the Al/Ga column with that on the As column. Does this require better spatial resolution than the authors have available?

Authors: The experimental images, shown in our companion paper, show that there is a difference in intensities at the positions of the two atomic columns although the two columns are not resolved. Thus comparing intensities at two points within the image of a pair of columns gives a better estimation of the aluminium concentration than does the intensity at the midpoint between the columns. In this paper, which is more concerned with numerical methods, we have chosen to examine the intensity at just a few points.

A Howie: Provided the local specimen thickness is known (e.g., from plasmon losses), the HAADF signal averaged over the unit cell would give a simple measure of the Al content. Are the authors able to make any comment about this low resolution approach compared with their methods, the high resolution method mentioned in the previous question or some of the other methods used to address this problem (e.g., measurement of 002 dark field image intensities)? Might there not be some merit in trying as many as possible of these methods for comparison on a single specimen?

Authors: We agree that reliance should not be placed on one technique and we discuss some other techniques in the companion paper. The average intensity will give an estimate of aluminium content but this method is sensitive to local thickness which is difficult to determine to an accuracy of one or two unit cells.

A Howie: It is not entirely clear how absorption has been treated in these computations. Am I correct in assuming that the absorption potential used has a TDS part which serves to normalise the "elastic" scattering in the frozen phonon model, i.e., to keep the total intensity unity in the absence of inelastic scattering and an inelastic part, due to electronic excitations (including plasmons?), which generates the term multiplying β in equation (16)?

Authors: We hope that our revised paper has cleared up how absorption is treated. The computations include only absorption due to thermal diffuse scattering while we make a comment on inelastic scattering due to single electron excitation at the end. Plasmons are not included. It is expected that electrons that have lost energy due to plasmon excitation make contributions to the image which are similar to those electrons which have not lost energy since the angles of scattering associated with the energy loss are very small.

A. Howie: In the single, large angle scattering approximation, integration over the detector acceptance angles produced substantial cancellation of the interference between pairs of atoms unless they share

the same rather small coherence volume. It is this effect which incidentally probably makes HAADF imaging more sensitive than other imaging modes to the correlated thermal motion of neighbouring atoms. When, as in the authors' work, multiple large angle scattering events are considered there might be an even greater advantage in not leaving all of the angular integrations until the last stage of the computation. Do the authors think that this might be possible?

S. J. Pennycook: At large thicknesses the convergent beam discs contain fine scale interference details which must be accurately integrated to give the detected signal. Since these individual interference features do not contribute to the integrated intensity, could a further gain in computational efficiency be obtained by taking the intensity at real space at each atomic site and summing over sites? One might anticipate that provided the inner radius of the detector was reasonably large, one could simply assign an effective scattering cross section to each atom. This would also build in the Einstein model of thermal vibrations that is simulated by the frozen lattice model. It might also prove necessary only to include the number of Fourier components sufficient to represent the thermally smeared atomic potential.

Authors: One could, for instance, assign to each atom a scattering function which depends on the parameters of the detector. The total intensity would then be found by summing over all scattering functions multiplied by the local intensity of the elastic wave. This is an approximation which can be readily tested and represents an extension of the work of Pennycook and Jesson (1991) who assumed the scattering functions are delta functions. The atomic scattering function could be obtained by computing intensity of an image of a single atom. While not delta functions, these scattering functions would still be sharply peaked and thus have a large number of Fourier components.

C. Dinges and H. Rose: The authors should compare the result for the image intensity obtained by the use of equations 13 and 14 assuming a single atom, the Einstein model and ideal lens. Do they really obtain the same results? If not, what is different and how can the differences be explained?

Authors: We would expect to obtain the same results. We chose to test our method by comparing the intensities it predicts with those using the Monte Carlo approach.

C. Dinges and H. Rose: The authors performed their calculations on a 256 x 256 matrix assuming a small supercell. Hillyard and Silcox (1995) use a 512 x 512 matrix and a large supercell. Results published by Dinges et al. in these proceedings are based on the same matrix size and supercell size. The reason for choosing large supercells is to suppress periodic effects stemming from the FFT. The explanation of the authors to justify their small supercells should be more detailed.

Authors: We agree that the large supercell is more appropriate for analysing experimental images. We believe that the small supercell used in this paper is adequate for comparing different numerical methods. We have calculated how the value of the defocus which gives the sharpest probe depends on the size of the calculation and we found that for a 4 x 4 supercell it is -55 nm, for a 6 x 6 supercell it is -65 nm and for a 8 x 8 supercell it is -68 nm, close to the Scherzer value.

C. Dinges and H. Rose: It is not clear what is new in the theory given in the paper. Where is the difference between the multislice theory in this paper and the theories of Wang and of Dinges and Rose?

J. M. Gibson: If the frozen phonon method is more efficient and accurate than the alternative method proposed here, why bother to try it at all?

Authors: While all of these formulations are equivalent in a mathematical sense they differ somewhat in their derivations and hence one approach may bring out more clearly certain aspects of the underlying principles on which they are based. From the point of view of numerical calculations, the aim of formulating the problem of calculating thermal diffuse scattering in terms of a set of scattering functions is to provide a basis for generating a variety of approximations which involve substantially less computation but are sufficiently accurate.

J. M. Gibson: Could the authors be more clear about the complications of varying thickness in measuring composition? This is certainly an issue with HREM techniques.

Authors: The shape of the image does not change significantly over a change of thickness of a few unit cells so it is possible to obtain estimates of composition in foils which vary in thickness. Calculations by Anderson (1997) indicate that, to within 5%, the image intensity of a foil 0.8 nm thick is a constant fraction of the image intensity of a 8 nm-thick foil, which in turn is a constant fraction of a 16 nm thick foil to within 5%.

M. Hÿtch: The most critical test for the various simulation methods seems to be in the prediction of absolute intensities. Is it possible to calibrate experimental HAADF images, i.e. with respect to the incident intensity? The proposed method of estimating β from point A in an experimental image of a thin foil would also seem to rely on such a calibration.

Authors: β is a parameter used for comparing the results of computations because it involves the intensity due to elastic scattering. Since energy filters cannot remove thermal diffuse scattering, β is not accessible to experiment. The calibration of experimental intensities is complicated by the processing carried out by the

microscope's image acquisition system which is adjusted to obtain high contrast. The use of annular detectors for quantitative measurements is discussed by Kirkland and Thomas (1996).

Additional References

Anderson SC (1997) Electron Optical Approaches to Quantitative Compositional Measurement at High Spatial Resolution. Doctoral Thesis, The University of Sydney.

Hillyard S, Silcox J (1995) Detector geometry, thermal diffuse scattering and strain effects in ADF STEM imaging. Ultramicroscopy **58**: 6-17.

Kirkland EJ, Thomas MG (1996) A high efficiency annular dark field detector for STEM. Ultramicroscopy **62**: 79-88.